Supporting Information for

Kesterite Cu_2ZnSnS_4 as a Low Cost Inorganic Hole Transporting Material for High Efficiency Perovskite Solar Cells

*Qiliang Wu, Cong Xue, Yi Li, Pengcheng Zhou, Weifeng Liu, Jun Zhu, Songyuan Dai, Changfei Zhu, and Shangfeng Yang**

[a] *Hefei National Laboratory for Physical Sciences at Microscale, Key Laboratory of Materials for Energy Conversion, Chinese Academy of Sciences, Department of Materials Science and Engineering, Synergetic Innovation Center of Quantum Information & Quantum Physics, University of Science and Technology of China (USTC), Hefei 230026, China.*
[b] *Key Laboratory of Novel Thin Film Solar Cells, Hefei Institutes of Physical Science, Chinese Academy of Sciences, Hefei 230031, China.*

Contents

S1. TEM images of CZTS nanoparticles.

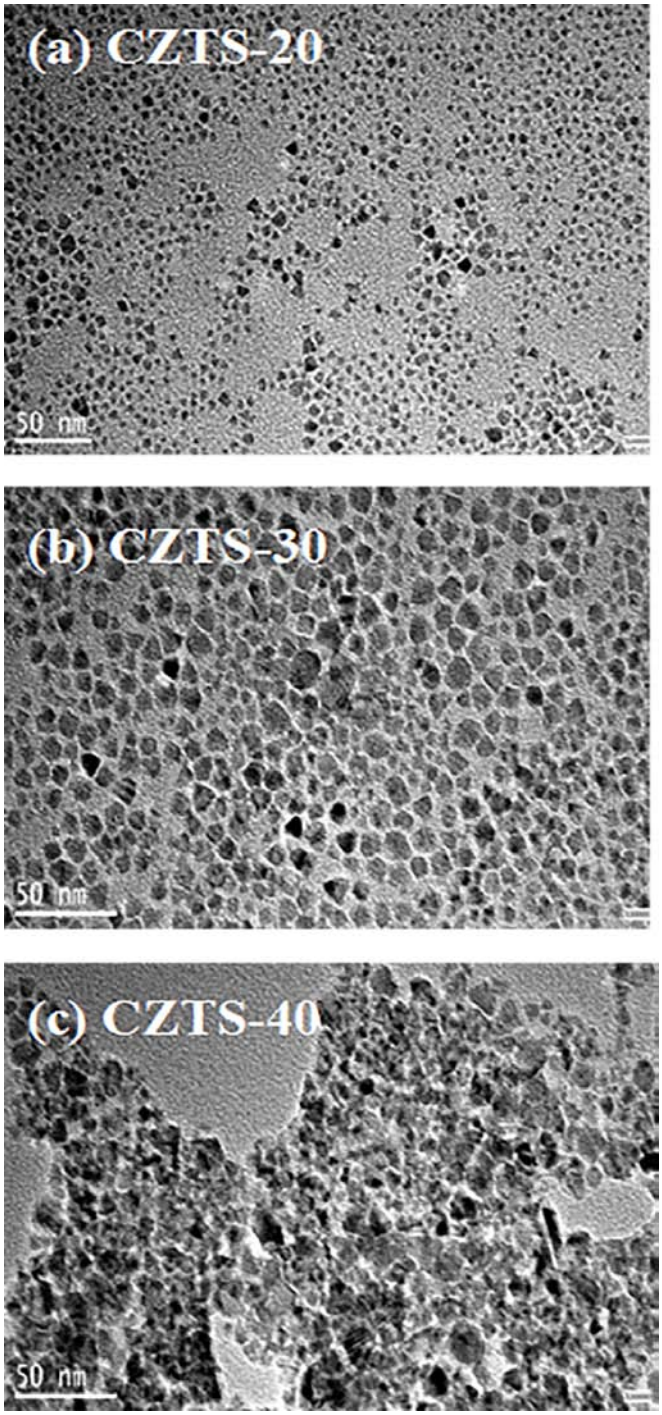

Figure S1. TEM images of CZTS nanoparticles synthesized with reaction time of 20 (a), 30 (b) and 40 (c) minutes, abbreviated as CZTS-20, CZTS-30 and CZTS-40 respectively.

S2. Optimization of the size, spin-coating speed and annealing time of CZTS nanoparticals and dispersion solvent.

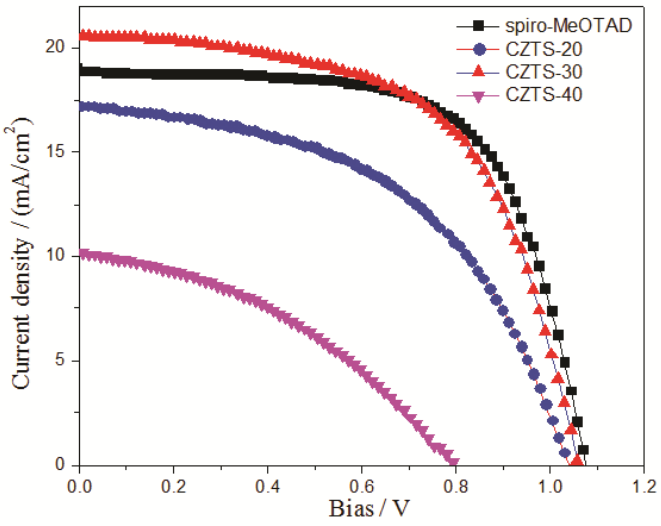

Figure S2. J-V curves of $CH_3NH_3PbI_3$ PSC devices based on CZTS nanoparticals with different sizes or spiro-OMeTAD HTM measured under illumination of an AM 1.5 solar simulator (100 mW cm^{-2}) in air.

Table S1. Photovoltaic parameters of the best FTO/TiO_2/$CH_3NH_3PbI_3$ perovskite/HTM/Au PSC devices with different HTMs.

Hole transport material (HTM) [a]	Reaction time (min)	V_{oc} (V)	J_{sc} (mA/cm^2)	FF (%)	PCE (%)
CZTS-20	20	1.04	17.20	50.1	8.94
CZTS-30	30	1.06	20.54	58.7	12.75
CZTS-40	40	0.80	10.16	38.6	3.12
spiro-MeOTAD	-	1.07	18.94	65.0	13.23

[a] Annealing temperature is fixed at 100 ^oC.

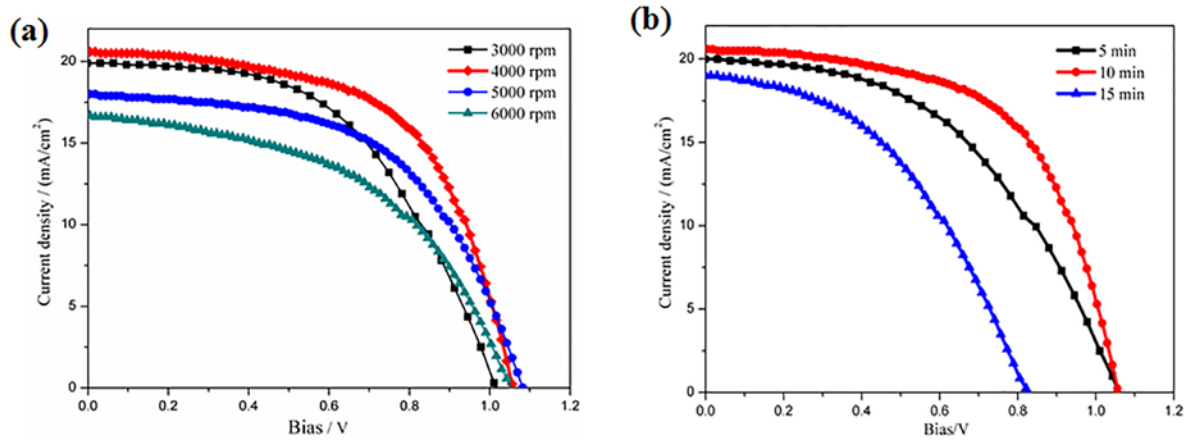

Figure S3. J-V curves of $CH_3NH_3PbI_3$ PSC devices with CZTS-30 HTM prepared with different spin-coating speeds (a) and annealing times (b). The measurements were carried out under illumination of an AM 1.5 solar simulator (100 mW cm^{-2}) in air.

Table S2. Photovoltaic parameters of the best $CH_3NH_3PbI_3$ PSC devices based on CZTS-30 HTM prepared with different spin-coating speeds and annealing times.[a]

spin-coating speed (rpm)	annealing time (min)	V_{oc} (V)	J_{sc} (mA/cm^2)	FF (%)	PCE (%)
3000 [b]	10	1.02	19.91	51.7	10.51
4000 [b]		1.06	20.54	58.7	12.75
5000 [b]		1.08	17.98	55.2	10.73
6000 [b]		1.05	16.72	49.1	8.61
4000	5 [c]	1.06	20.00	47.8	10.10
	10 [c]	1.06	20.54	58.7	12.75
	15 [c]	0.83	19.02	43.9	6.89

[a] Annealing temperature is fixed at 100 °C. [b] Annealing time is fixed at 10 min. [c] Spin-coating speed is fixed at 4000 rpm.

Table S3. Photovoltaic parameters of the $CH_3NH_3PbI_3$ PSC devices based on CZTS-30 HTM dispersed in chlorobenzene with different spin-coating speeds.

spin-coating speed (rpm)	annealing time (min)	V_{oc} (V)	J_{sc} (mA/cm^2)	FF (%)	PCE (%)
2000	10	0.81	1.82	32.59	0.48
3000		0.93	6.48	34.64	2.09
4000		0.86	3.46	44.78	1.34

S3. Histograms of PCE, J_{sc} and FF.

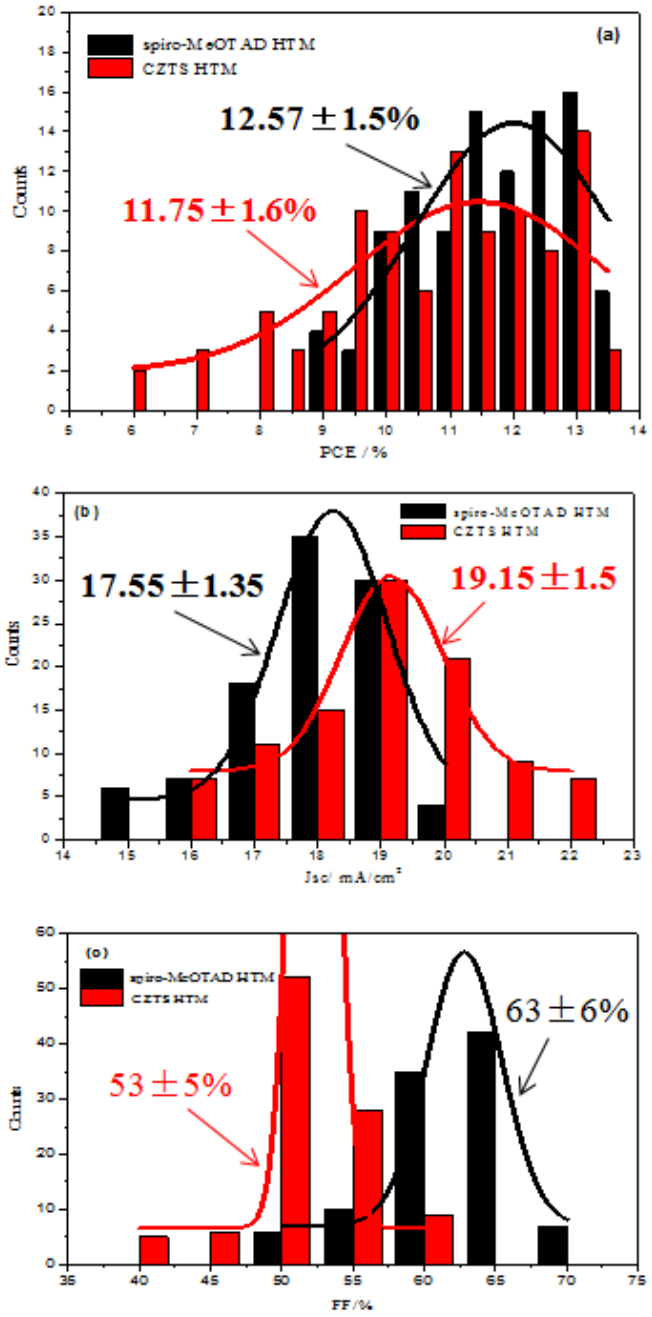

Figure S4. Histograms of PCE (a), J_{sc} (b) and FF (c) for the $CH_3NH_3PbI_3$ perovskite-based PSCs devices with different HTMs.

S4. Hysteresis of J-V curves of the devices with different HTMs.

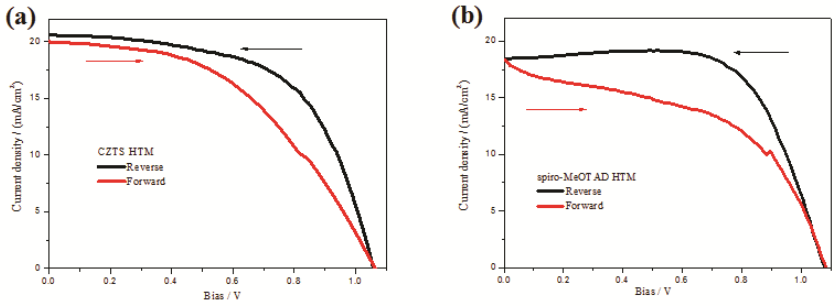

Figure S5. J-V curves of $CH_3NH_3PbI_3$ PSCs devices with CZTS (a) and with spiro-OMeTAD (b) HTM in different scan directions. The measurements were carried out with 0.1 V/s scan rate under AM 1.5 illumination at an irradiation intensity of 100 mW·cm^{-2}.

Table S4. Photovoltaic parameters of the best FTO/TiO_2/$CH_3NH_3PbI_3$ perovskite/HTM/Au PSC devices with different HTMs in different scan directions with 0.1 V/s scan rate.

HTM	Scan direction	V_{oc} (V)	J_{sc} (mA/cm^2)	FF (%)	PCE (%)	Hystersis of PCE [a]
CZTS	Reverse	1.06	20.54	59.7	12.75	22.4%
	Forward	1.06	19.94	46.7	9.90	
spiro-MeOTAD	Reverse	1.08	18.51	67.6	13.51	28.3%
	Forward	1.08	18.49	48.5	9.69	

[a] Hystersis of PCE = [PCE(reverse) - PCE(forward)]/PCE(reverse)

S5. Stabilized power output for the devices with different HTMs.

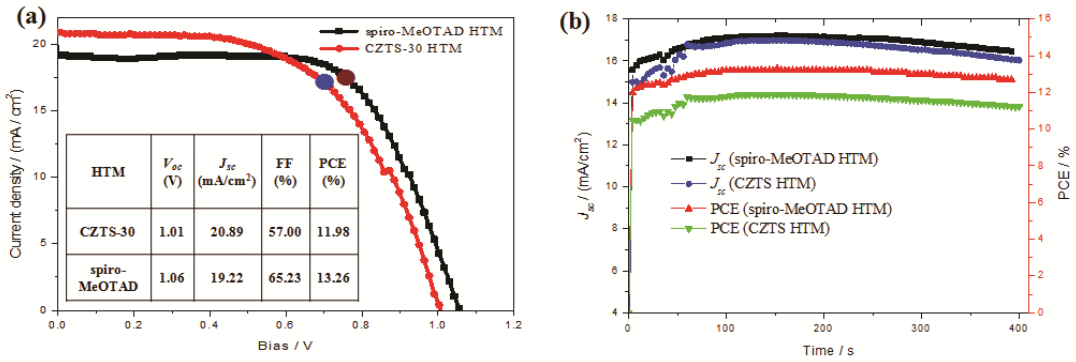

Figure S6. (a) J-V curves of $CH_3NH_3PbI_3$ PSC devices with CZTS-30 or spiro-MeOTAD HTM measured under illumination of an AM 1.5 solar simulator (100 mW cm^{-2}) in air. The maximum power point is 0.70 and 0.76 V for CZTS-30 and spiro-MeOTAD, respectively. (b) Photocurrent density (J_{sc}) and power conversion efficiency (PCE) as a function of time for the device held at 0.70 V (CZTS) or 0.76 V (spiro-MeOTAD) forward bias.

S6. PL spectra of $CH_3NH_3PbI_3$ perovskite films coated by CZTS nanoparticles.

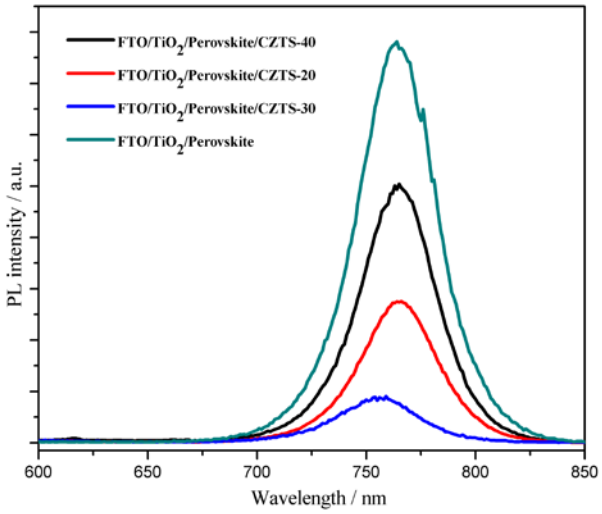

Figure S7. PL spectra of $CH_3NH_3PbI_3$ perovskite films with and without CZTS nanoparticles with different sizes.

S7. AFM images of the perovskite/CZTS and perovskite/spiro-MeOTAD films.

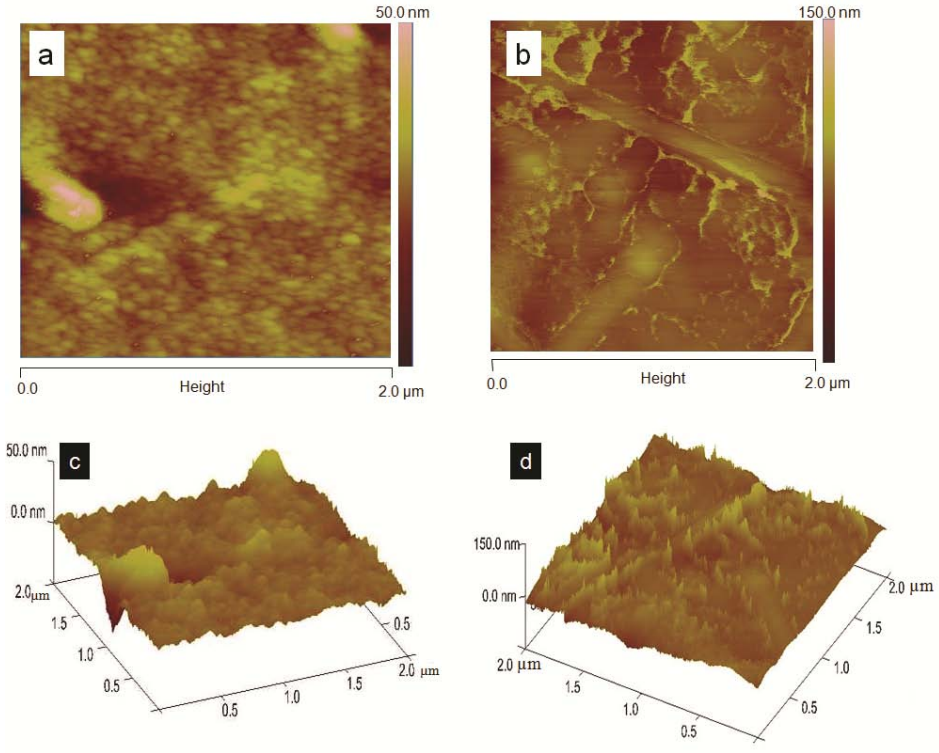

Figure S8. 2D and 3D AFM images of the perovskite/CZTS (a, c) and perovskite/spiro-MeOTAD (b, d) films.

S8. XRD patterns of $CH_3NH_3PbI_3$ perovskite films with or without CZTS HTM.

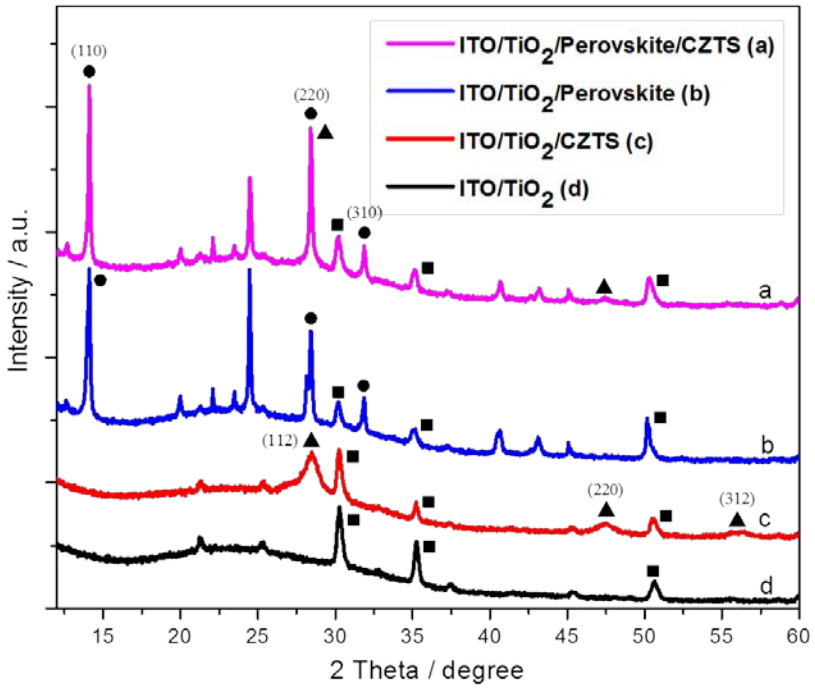

Figure S9. XRD patterns of $CH_3NH_3PbI_3$ perovskite films with or without CZTS film. The filled circle, triangle and square mark the characteristic diffraction peaks of $CH_3NH_3PbI_3$ perovskite, CZTS and TiO_2, respectively.

S9. Impedance spectra of the devices under different biases.

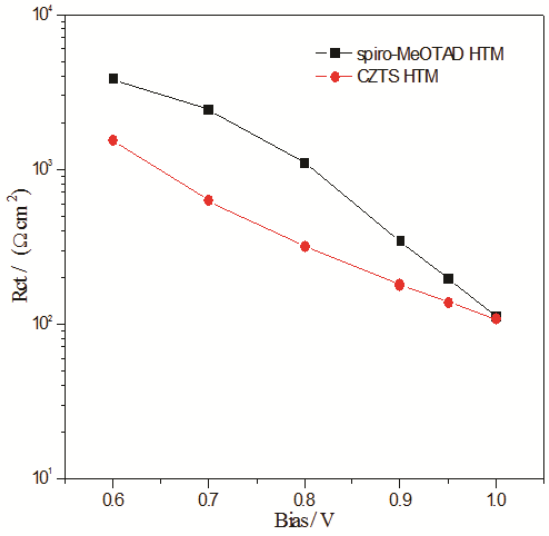

Figure S10. Recombination resistance (R_{rec}) of the devices with different HTMs at different biases.